J Mater Sci (2011) 46:534–540
DOI 10.1007/s10853-010-5000-8

Mechanical performance and cellulose microfibrils in wood with high S2 microfibril angles

Ping Xu · Huawu Liu · Lloyd A. Donaldson · Yi Zhang

Received: 3 June 2010 / Accepted: 9 October 2010 / Published online: 28 October 2010

Abstract Corewood and compression wood, both with high S2 microfibril angles, are the worst parts of the tree most in need of improvement in wood quality. This study focuses on the characteristics of cellulosic reinforcement in wood with high S2 microfibril angles lying between 35° and 60°, as well as the probable influence of these characteristics on wood longitudinal mechanical properties. Stiffness and tensile strength were measured on 221 thin radiata pine wood strips. The results indicate that at high angles, the average values of wood stiffness and tensile strength are low with relatively large variations. The variations of stiffness and strength are weakly correlated with the variation of S2 microfibril angles, regardless of wood type. Further study involved examining the characteristics of cellulose microfibrils within the S2 layer using dual axis electron tomography for samples with the same microfibril angle but differing mechanical performance. From the fact that the severe compression wood possessed fewer cellulose microfibrils and had abundant dislocations, and that at many kinking points these cellulose microfibrils were broken down into shorter dislocation segments, it was concluded that the characteristics of cellulose microfibril reinforcement are responsible for the inferior stiffness and tensile strength in the severe compression wood compared with normal corewood with the same high S2 microfibril angle.

P. Xu (✉)
Scion, P.O. Box 29237, Christchurch 8540, New Zealand
e-mail: ping.xu@scionresearch.com

H. Liu · Y. Zhang
Tianjin Polytechnic University, 63 Chenglin Road, Tianjin 300160, People's Republic of China

L. A. Donaldson
Scion, Private Bag 3020, Rotorua 3046, New Zealand

Introduction

The wood cell wall is a natural anisotropic composite in which cellulose microfibrils are embedded as reinforcing material in a matrix of lignin-hemicellulose. The mechanical performance of wood fibres, in particular, Young's modulus in the fibre longitudinal direction (fibre axial stiffness) and tensile strength, largely depend on the properties of cellulose microfibrils located in the S2 layer, the spatial angle between the cellulose microfibrils and the longitudinal axis of the wood cell wall (usually called S2 microfibril angle), and how the cellulose microfibrils acting as reinforcement are embedded in the lignin-hemicellulose matrix (bundling of cellulose microfibrils) [1–5]. Research has focused on the size of a single cellulose microfibril [6–8]; the cellulose microfibril angle of the S2 layer in individual wood fibres or in small clears [9–11]; and the effects of microfibril angle on wood quality, especially wood stiffness [2, 12–15].

While cellulosic reinforcement is acknowledged as a key factor dominating wood longitudinal mechanical properties, a question has arisen regarding the role of the properties of cellulose microfibrils on fibre axial stiffness and strength at high microfibril angles. Mark and Gillis [12] assumed that, when S2 microfibril angle lies between 25° and 50° there is little variation of fibre axial stiffness; and at high S2 angles (>25°) fibre axial stiffness is insensitive to the properties of cellulosic reinforcement but depends on the properties of the lignin–hemicellulose matrix, whereas others suggested that the fibre longitudinal modulus is not affected by variations in either the

hemicelluloses or the lignin properties, since the properties of lignin and hemicelluloses mainly contribute to fibre transverse modulus rather than fibre axial stiffness [4, 5]. Some authors claimed that the spacings between cellulose microfibrils might be important in determining the elastic properties of wood cell walls [16]. However, few attempts have been made to determine the bundling of cellulose microfibrils within the S2 layer of wood cell walls at high angles. All these studies demand knowledge regarding the characteristics of cellulosic reinforcement in high angle wood as well as the probable influence of these characteristics on wood axial mechanical properties.

Corewood and compression wood generally have high microfibril angles. It has been reported that the S2 microfibril angle in individual tracheids could be as high as 55° for normal corewood in New Zealand radiata pine [17]. Our research interest is the corewood and compression wood with S2 angles larger than 35°, since such wood is the worst part of the tree and is most in need of improvement. More financial benefit could be gained in seeking to improve the worst properties rather than properties that are already adequate [18].

In this study, we measured longitudinal Young's modulus (stiffness) and tensile strength of thin wood strips at high angles (>35°), and also examined the characteristics of cellulosic reinforcements embedded in the lignin–hemicellulose matrix for samples with the same S2 microfibril angle but significantly different mechanical properties.

Samples and methods

Preparation overview

Wood samples were collected from the corewood of a 17-year-old radiata pine butt log. Prior to mechanical testing, matchstick-sized specimens were prepared to assess the average values of microfibril angles using polarised light microscopy [17]. The wood type was then examined in terms of normal wood and severe compression wood using autofluorescence of lignin [19]. A total of 236 thin wood strips were cut from 23 wood samples with high angles (>35°) for mechanical testing. After mechanical testing, small blocks were cut from the samples that had the same values for S2 microfibril angle but significantly different values for stiffness and tensile strength. Reconstruction of cell walls was then undertaken from these blocks using 3D dual-axis tomography.

Stiffness and strength in tension

In order to measure wood mechanical properties at the fibre level, wood strips with small dimensions were prepared (Fig. 1a). The length of each thin strip was oriented along the longitudinal axis of the grain. All wood strips were air-dried to 12% MC.

Stiffness and tensile strength of wood strips were measured using an INSTRON tensile tester (50-kN capacity) with a load cell capacity of 0–100 N in a conditioned room (RH 65% ± 2; temperature 20 ± 2 °C). To avoid any slippage between the thin wood strip and the pneumatic clamps of the tensile tester, two cardboard frames were glued to the ends of each thin strip with a 10-mm distance between the frames (Fig. 1b). The cardboard frames were held by the clamps, and a computer system automatically recorded the applied uniaxial forces, strains and the maximum force at the failure point.

Reconstruction of wood cell walls

Wood blocks prepared for reconstruction of cell walls were dehydrated in an acetone series, embedded in Spurr resin and sectioned at 150-nm thickness in the transverse plane using a diamond knife. The sections were placed on copper slot grids on a formvar support film and stained with 2% potassium permanganate in 2% sodium citrate solution for 5 min followed by washing in water. After staining, gold particles (10 nm in diameter) were applied to both sides of each specimen as fiducials, and the specimens were coated

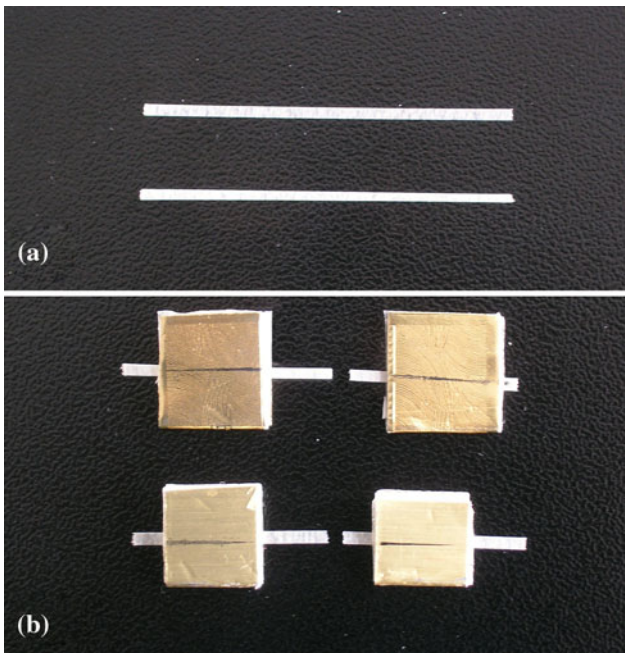

Fig. 1 **a** A total of 236 thin wood strips with dimensions of 2 × 0.2 × 30 mm^3 (width × thickness × length) were prepared to measure stiffness and tensile strength. **b** The broken wood strips after tensile testing

with a carbon support film using a BAL-TEC Med020 high vacuum coating system.

A 300-kV transmission electron microscope (TF 30) was used to collect raw stacks using dual-axis tilting. The specimen was tilted in the microscope from −60° to +60° with 1° intervals. When the first tilt series was completed around axis A, the specimen was then rotated 90° and a second tilt series was collected around axis B. A magnification of 39,000× with a binned pixel size of 0.63 nm was used for the severe compression wood specimens, and a magnification of 59,000× with a binned pixel size of 0.41 nm was used for the normal wood specimens. The updated IMOD software package developed by the Boulder Laboratory for 3D Electron Microscopy [20] was used to process the raw stacks and reconstruct the cell walls. The *3dmod* software package [21] was then used to track and map the cellulose microfibrils in the reconstructed wood cell walls as described by Xu et al. [8]. To ensure that the observed samples do not have damage generated by the cutting force of the diamond knife, 40 tomographic slices that were close to the cut surfaces of the section were excluded from the analysis.

Results and discussion

Stiffness and tensile strength in wood with high angles

After excluding 15 wood strips that failed at the clamps, the remaining 221 thin wood strips were analysed to get average values of stiffness and tensile strength for the 23 high angle wood samples.

Figure 2 shows the variation of average values of stiffness at high angles. When microfibril angle falls in the range of 35°–60°, the average values of stiffness are low in general, and the variation of stiffness is weakly correlated with the variation of microfibril angle for all sample points ($R^2 = 0.1445$), regardless of wood type. A further analysis shows a weak relationship for both normal corewood and severe compression wood samples ($R^2 = 0.3574$ and 0.1434, respectively).

Figure 3 indicates the profile of the average values of tensile strength in the same high angle range shown in Fig. 2. Similar to the stiffness performance, the average values of tensile strength are low in general, and the variation of tensile strength is weakly correlated with the variation of S2 angle in all situations ($R^2 = 0.2626$, 0.3349 and 0.3990, respectively).

It is not unexpected that the variations of wood longitudinal mechanical properties are weakly correlated to the variation of S2 microfibril angle at high angles shown in Figs. 2 and 3. When a uniaxial tensile load is applied on wood cell walls (fibres), because of S2 microfibril angle,

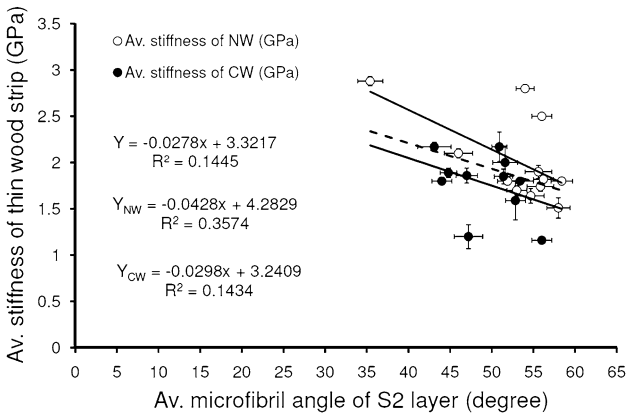

Fig. 2 Average values of wood longitudinal Young's modulus (stiffness) in normal corewood (NW) and severe compression wood (CW) at high S2 microfibril angles between 35° and 60°. For each sample point, 25 tracheids were measured to determine an average value of microfibril angle, and at least 8 thin wood strips were tested to determine an average value of stiffness. The *error bar* along the *X* direction indicates ±standard error of average microfibril angle, and the *error bar* along the *Y* direction indicates ±standard error of average stiffness

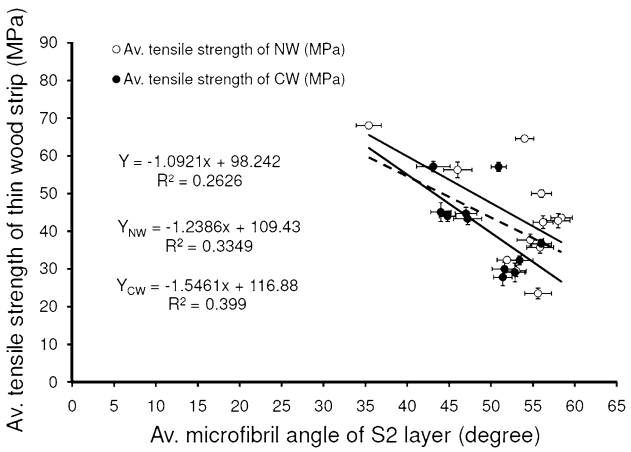

Fig. 3 Average values of wood tensile strength in normal corewood (NW) and severe compression wood (CW) at high S2 microfibril angles between 35° and 60°. For each sample point, 25 tracheids were measured to get an average value of microfibril angle, and at least 8 thin wood strips were tested to get an average value of tensile strength. The *error bar* along the *X* direction indicates ±standard error of the average microfibril angle, and the *error bar* along the *Y* direction indicates ±standard error of the average tensile strength

the longitudinal axis of the wood cell wall (fibre) does not coincide with the longitudinal axis of cellulose microfibrils embedded in the S2 layer. This means that the tensile stress applied on cell walls results in not just longitudinal strain of individual cellulose microfibrils but also transverse strain and longitudinal–transverse shear strain in these cellulose microfibrils, as well as a shear strain of the lignin–hemicellulose matrix between the cellulose microfibrils. For a wood strip containing several fibres, there is

also a shear strain of the lignin–hemicellulose matrix between fibres. When S2 microfibril angle increases, the contribution of the elastic modulus of cellulose microfibrils to fibre axial stiffness reduces, whereas the effect of the lignin–hemicellulose matrix increases due to shear. When the S2 angle is larger than a certain value, shears become significant [22–25]. In this case, the variation of microfibril angle is no longer sensitive to the variation of wood axial stiffness. Therefore, there are poor relationships between wood stiffness and S2 angles shown in Fig. 2. A similar concept can be applied to explain the weak relationships between the tensile strength and S2 angles shown in Fig. 3.

Cellulose microfibrils are much stiffer and stronger than the lignin–hemicellulose matrix in which the cellulose microfibrils are embedded; and "The chemical substances that comprise the matrix would not be expected to behave elastically or provide much stiffness because of their branched, short-chain nature" [12]. When the contribution of stiff and strong cellulose microfibrils to wood longitudinal mechanical properties is largely reduced, it is not surprising that the average stiffness and strength present low values as shown in Figs. 2 and 3. However, differing from the model of Mark and Gillis [12], our experimental results shown in Figs. 2 and 3 indicate a relatively large variation of stiffness and tensile strength at high angles. With the increase of S2 angle from 35° to 60°, the average values of stiffness vary from 2.88 to 1.51 GPa in normal corewood, and from 2.17 to 1.16 GPa in severe compression wood; the average values of tensile strength vary from 68.1 to 23.5 MPa in normal corewood, and from 57.2 to 27.8 MPa in severe compression wood. Such large variation of longitudinal mechanical properties is unlikely to be caused by the lignin–hemicellulose matrix which has low and relatively stable axial stiffness and strength properties. Most interesting is that some points shown in Figs. 2 and 3 have very similar values for S2 microfibril angle but show quite different performances for stiffness and tensile strength. Therefore, further tests were used to determine the characteristics of cellulose microfibril reinforcements embedded within the S2 layer at high angles.

Cellulose microfibrils per square nanometre

The term "cellulose microfibrils per square nanometre" is defined in this study as the number of cellulose microfibrils per square nanometre as seen in transverse sections of a cell wall.

Figures 4, 5 and 6 are tomographic slice images produced in this study. Since heavy metal stains are excluded from the crystalline core of cellulose microfibrils [3, 26–28], the white structures shown in the tomography images correspond to the non-stained core region of individual cellulose microfibrils [8, 26, 28], whereas the dark grey and black structures correspond to the stained lignin and hemicellulose matrix [8, 26, 28–30]. The individual cellulose microfibrils have a diameter of approximately 2.1 nm [6, 8], and the larger white structures are suggested to represent clusters of cellulose microfibrils [8, 31–33]. The white arrows shown in Figs. 4 and 5 indicate examples of single cellulose microfibrils; the black arrows shown in Figs. 4 and 5 indicate an example of clusters of cellulose microfibrils; and the white boxes shown in Figs. 4 and 5 indicate the selected regions used for determining the cellulose microfibrils per square nanometre.

Figure 4 is a tomographic slice image showing the inner part of a cross-section of the S2 layer from a severe compression wood sample. This compression wood sample had a S2 microfibril angle of 56°, a stiffness of 1.16 GPa and a tensile strength of 36.7 MPa as shown in Figs. 2 and 3. Figure 5 shows the inner part of a cross-section of the S2 layer from a normal corewood sample that had the same S2 microfibril angle value (56°) but a stiffness of 2.5 GPa and strength of 50 MPa as shown in Figs. 2 and 3. Eight regions with similar dimensions were selected, and non-stained cores of cellulose microfibrils were tracked throughout the reconstructed slice images to determine the cellulose microfibrils per square nanometre. Figure 6 is an enlarged tomographic slice image showing an example of the sample regions illustrated in Fig. 4.

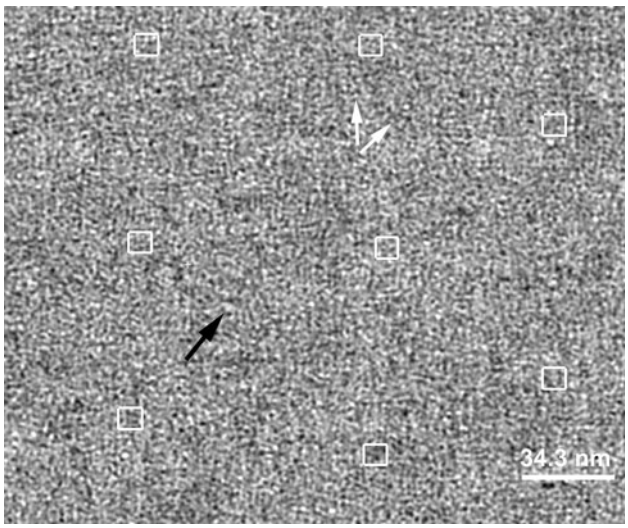

Fig. 4 Tomographic slice image (1-nm thick) of the inner part of a cross-section of the S2 layer from a severe compression wood sample that had a microfibril angle of 56°, a stiffness of 1.16 GPa and a tensile strength of 36.7 MPa as shown in Figs. 2 and 3. Eight regions were selected to examine the cellulose microfibrils per unit of cell wall area. The *white arrows* show examples of single cellulose microfibrils; the *black arrow* indicates an example of clusters of cellulose microfibrils; and the *white boxes* indicate the selected regions used for determining the cellulose microfibrils per square nanometre

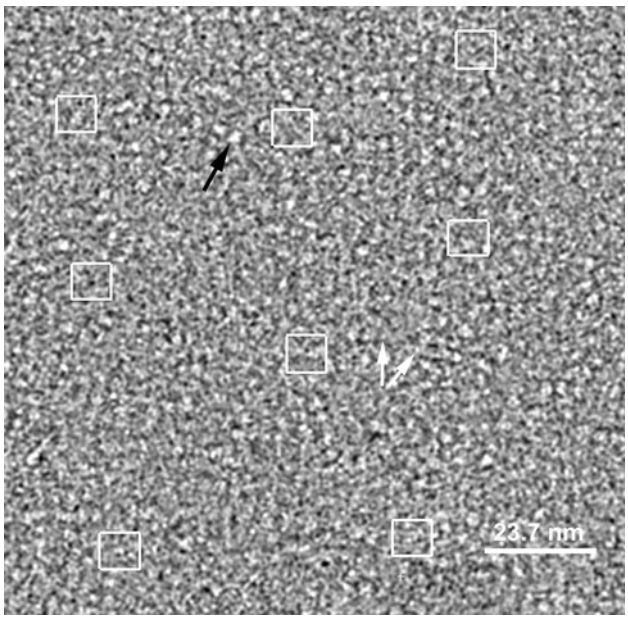

Fig. 5 Tomographic slice image (1-nm thick) of the inner part of a cross-section of the S2 layer from a normal corewood sample that had the same microfibril angle as the specimen shown in Fig. 4 but a stiffness of 2.5 GPa and a tensile strength of 50 MPa. Eight regions were selected to examine the cellulose microfibrils per unit of cell wall area. The *white arrows* show examples of single cellulose microfibrils; the *black arrow* indicates an example of clusters of cellulose microfibrils; and the *white boxes* indicate the selected regions used for determining the cellulose microfibrils per square nanometre

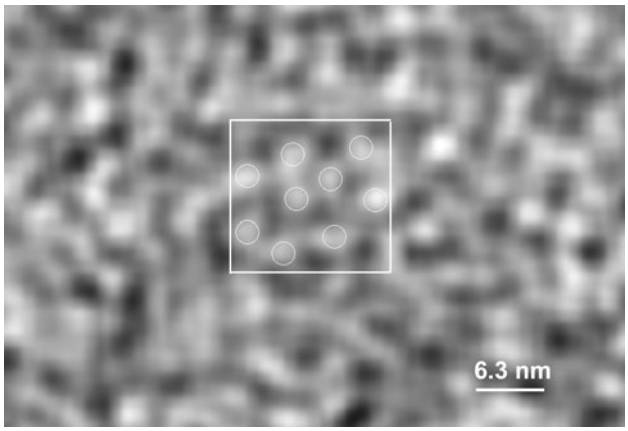

Fig. 6 Enlarged tomographic slice image of the inner part of the cross-section of a S2 layer showing an example of the selected regions illustrated in Fig. 4. The rectangle has an area of 63.6 nm^2 with a width of 8.19 nm and a height of 7.77 nm and contains nine cellulose microfibrils that are marked using *circles*

Our results show 0.208 cellulose microfibrils/nm^2 on average in the normal corewood specimen, but only 0.120/nm^2 on average in the severe compression wood specimen (Fig. 7). Mechanical properties of composites are affected by the amount, the length and the orientation of fibre reinforcements embedded in the composites [34]. We therefore suggest that the reduced number of cellulose microfibrils in the S2 layer may partly account for the inferior stiffness and tensile strength of compression wood when compared to normal corewood with the same microfibril angle. The length effect is discussed in following section.

Continuity of cellulose microfibrils

Once we know the number of cellulose microfibrils per unit cell wall area, it is important to understand how these cellulose microfibrils are embedded in the matrix of lignin–hemicellulose. We used small white cylinders to simulate the non-stained cores of individual cellulose microfibrils shown in Figs. 4 and 5, and tracked 76 tomographic slice images to examine the cellulose microfibrils from different orientations. Each white cylinder has a cross section of 2 nm in diameter to represent the non-stained core, and 1 nm thickness corresponding to the thickness of each tomographic slice image. These models allow us to assess the continuity of individual cellulose microfibrils by tracking the white cylinders through the series of slice images. The models are shown in Fig. 8 at different orientations.

From Fig. 8, one can see that the cellulose microfibrils are kinked along their length, and at many kinking points the cellulose microfibrils appear to be broken into short dislocated segments. Similar results have been observed in the tension wood of young poplar trees where kinked cellulose microfibrils with a maximum segment length of 40–50 nm were described [35].

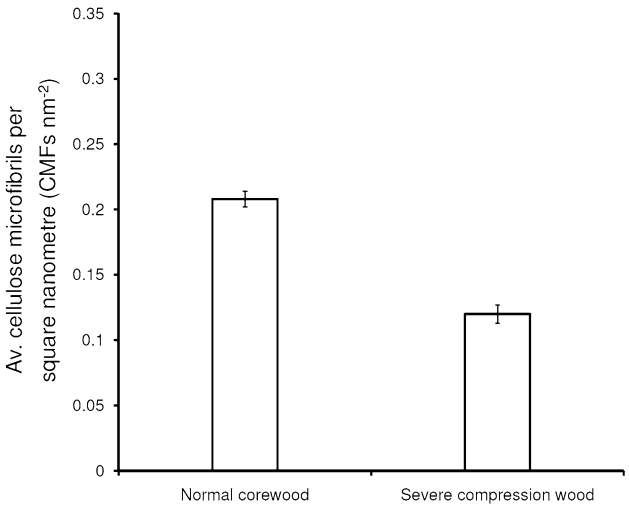

Fig. 7 The average values of cellulose microfibrils per square nanometre in the inner parts of the S2 layers shown in Figs. 4 and 5. The *error bar* along the *Y* direction indicates ±standard error of the cellulose microfibrils per square nanometre

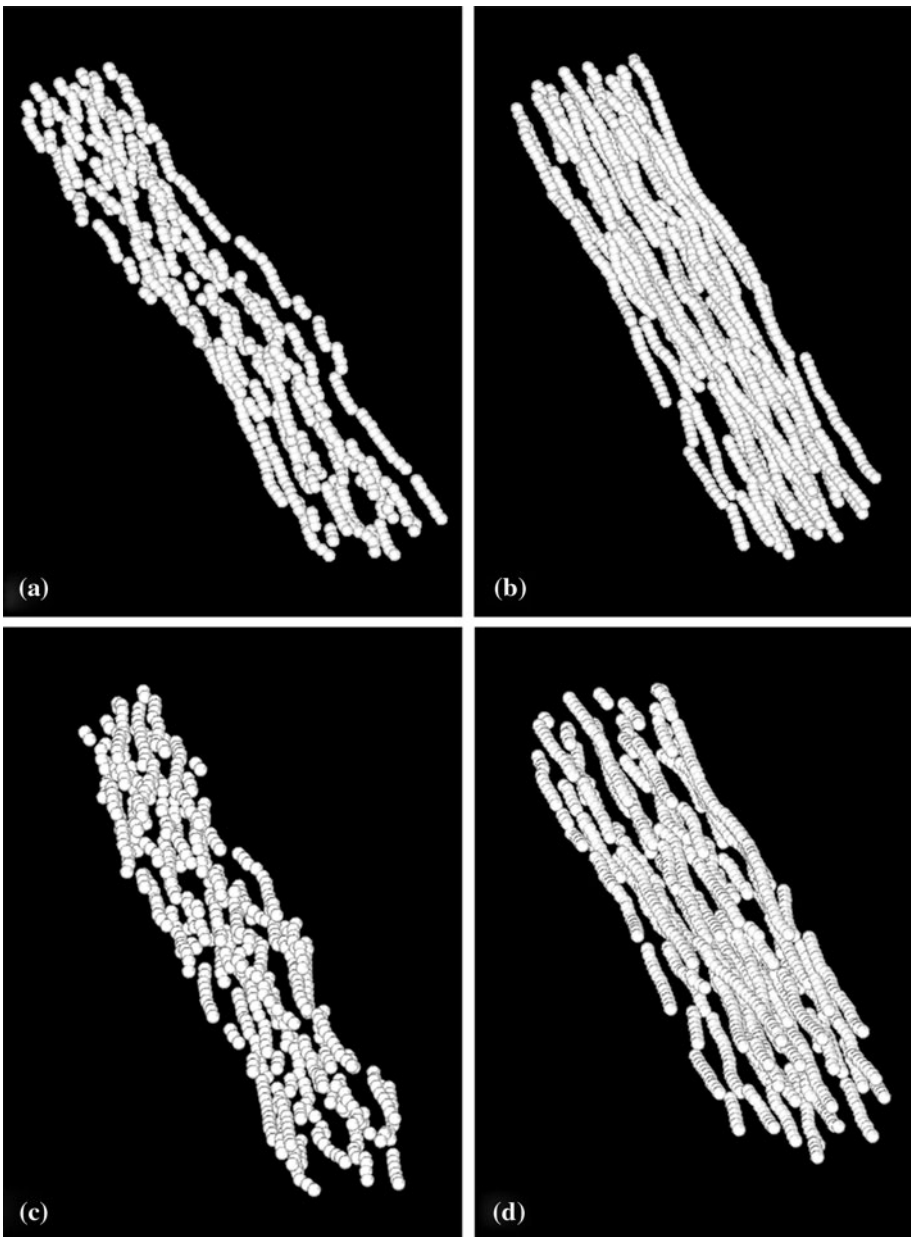

Fig. 8 **a** Model of the cellulose microfibrils obtained from 76 tracked tomographic slice images of the inner S2 layer in the severe compression wood cell wall shown in Fig. 4. **b** Model of the cellulose microfibrils obtained from 76 tracked tomographic slice images of the inner S2 layer in the normal wood cell wall shown in Fig. 5. The observation angles in **a, b** are: 70° (*X*-axis); 15° (*Y*-axis); 168° (*Z*-axis). **c**, **d** Models of the cellulose microfibrils shown in **a, b** are shown at a different orientation. The observation angles in **c**, **d** are: 43° (*X*-axis); 3° (*Y*-axis); −155° (*Z*-axis)

Dislocations of cellulose microfibrils observed in our study occur in the S2 layer of both the normal corewood and the severe compression wood samples but are more common in the S2 layer of the severe compression wood sample. This means that there are more weak points along the length of cellulose microfibrils in compression wood. Using IMOD software, we calculated the length of the dislocated segments of individual cellulose microfibrils. Within the 76 tracked tomographic slice images, the maximum length of the dislocated segments is 41.6 nm in the normal corewood sample but only 14.3 nm in the severe compression wood sample. Compared to the normal corewood sample with the same microfibril angle, it is clear that the more abundant dislocations and the shorter length of the cellulose microfibril segments contribute to reduce stiffness and tensile strength of the severe compression wood.

The exact nature of these dislocations is unknown. Some previous studies reported that cellulose microfibrils can be dislocated after lignin removal [36]. Delignification may also alter the aggregation of wood cellulose microfibrils [32, 37, 38]. However, the specimens used in this study were not delignified. Thus, the dislocations and the shorter segments observed in this study cannot be attributed to lignin removal. Previous studies have found that the corewood located at the base of a radiata pine stem had the

poorest stiffness [39] and the highest tendency to bow or crook [40]. We postulate that the dislocations observed in this study may reflect the inherent material characteristics of cellulose microfibrils from the base corewood of fast-grown trees.

Conclusions

At high S2 microfibril angles (>35°), wood stiffness and tensile strength presented low values and were poorly correlated to the variation of S2 microfibril angle, which can be attributed to reduced contribution of cellulose microfibrils and the increased effect of lignin–hemicellulose on wood longitudinal mechanical properties at high angles. When the S2 angle lies between 35° and 60°, the average values of stiffness and tensile strength showed relatively large variations in both normal corewood and compression wood. This is unlikely to be caused by variation of the lignin–hemicellulose matrix which has low and comparatively stable stiffness and strength properties.

Reconstruction of wood cell walls was completed in two samples that have the same S2 microfibril angle but quite different stiffness and tensile strength values. The tomographic slice images show that there are approximately 0.208 cellulose microfibrils/nm^2 of cell wall in the normal corewood sample but only 0.120/nm^2 in the severe compression wood sample. The tracked tomographic slice images show that, cellulose microfibrils are kinked in both normal corewood and severe compression wood samples with more abundant dislocations in the severe compression wood sample, and at many kinking points the cellulose microfibrils are broken down into dislocated segments. The maximum length of the dislocated segments is 41.6 nm in the normal corewood sample but only 14.3 nm in the severe compression wood sample. The characteristics of cellulose microfibril reinforcements observed in severe compression wood, such as lower number, abundant dislocations and shorter length, are suggested to be responsible for the inferior stiffness and tensile strength in severe compression wood compared with normal corewood with the same high S2 microfibril angle.

Acknowledgements We wish to thank the following contributors for their valued input to the project: Prof. David Mastronarde (Boulder Laboratory for 3-D Electron Microscopy of Cells, University of Colorado, USA) for his suggestions regarding trouble shooting of IMOD software; Dr. Jamie Riches (European Molecular Biology Laboratory, Germany) and Mr. Richard Walls (Agresearch, NZ) for collecting the raw image stacks by electron tomography; and Dr. Adya Singh (Scion, NZ) for his comments on the manuscript. The support of the New Zealand Foundation for Research, Science and Technology is also gratefully acknowledged.

References

1. Mark RE (1967) Cell wall mechanics of tracheids. Yale University Press, New Haven
2. Cave ID (1968) Wood Sci Technol 2:268
3. Preston RD (1974) The physical biology of plant walls. Chapman & Hall, London
4. Bergander A, Salmén L (2002) J Mater Sci 37:151. doi:10.1023/A:1013115925679
5. Salmén L (2004) Comptes Rendus Biol 327:873
6. Harada H, Goto T (1982) In: Brown RM (ed) Cellulose and other natural polymer systems: biogenesis structure and degradation. Plenum Press, New York, p 383
7. Jakob HF, Fengel D, Tschegg SE, Fratzl P (1995) Macromolecules 28:8782
8. Xu P, Donaldson LA, Gergely ZR, Staehelin LA (2007) Wood Sci Technol 41(2):101
9. Meylan BA (1967) For Prod J 17:51
10. Evans R (1999) Appita J 52:283
11. Donaldson LA (2008) IAWA J 29(4):345
12. Mark RE, Gillis PP (1973) Tappi 56(4):164
13. Cave ID, Walker JCF (1994) For Prod J 44(5):43
14. Evans R, Ilic J (2001) For Prod J 51(3):53
15. Nakada R, Fujisawa Y, Hirakawa Y (2003) Holzforshung 57:553
16. Tang RC, Hsu NN (1973) Wood Fiber 5(2):139
17. Donaldson LA (1992) NZ J For Sci 22:77
18. Walker J, Nakada R (1999) Int For Rev 1(4):251
19. Donaldson LA, Grace J, Downes GM (2004) IAWA J 25(3):253
20. Boulder Laboratory for 3-D Electron Microscopy of Cells (2009a) Tomography guide for IMOD version 3.13. http://bio3d.colorado.edu/imod. Accessed 28 April 2009
21. Boulder Laboratory for 3-D Electron Microscopy of Cells (2009b) Introduction to 3dmod version 3.13. http://bio3d.colorado.edu/imod. Accessed 28 April 2009
22. Köhler L, Spatz HC (2002) Planta 215:33
23. Keckes J et al (2003) Nat Mater Lett 2:810
24. Fratzl P, Burgert I, Keckes J (2004) Z Metallkd 95:579
25. Altaner CM, Jarvis MC (2008) J Theor Biol 253:434
26. Fromm J, Rockel B, Lautner S, Windeisen E, Wanner G (2003) J Struct Biol 143:77
27. Marchessault RH, Sundararajan PR (1983) Cellulose. In: Aspinall GO (ed) The polysaccharides, vol 2. Academic Press, New York, p 11
28. Kerr AJ, Goring DAI (1975) Cellulose Chem Technol 9(6):563
29. Hoffmann P, Parameswaran N (1976) Holzforschung 30:62
30. Sjöström E (1981) Wood chemistry: fundamentals and applications. Academic Press, New York
31. Awano T, Takabe k, Fujita M, Daniel G (2000) Protoplasma 212:72
32. Hult E-L, Larsson PT, Iversen T (2001) Polymer 42(8):3309
33. Åkerholm M, Salmén L (2002) J Pulp Paper Sci 28:245
34. Jones RM (1975) Mechanics of composite materials. Scripta Book Company, Washington, DC
35. Goto T, Harada H, Saiki H (1978) Wood Sci Technol 12:223
36. Nyholm K, Ander P, Bardage S, Daniel G (2001) Nordic Pulp Paper Res J 16:376
37. Duchesne I, Daniel G (2000) Nordic Pulp Paper Res J 15:54
38. Duchesne I, Hult E-L, Molin U, Daniel G, Iversen T, Lennholm H (2001) Cellulose 8:103
39. Xu P, Walker JCF (2004) Wood Sci Technol 38:1
40. Xu P, Liu H, Evans R, Donaldson LA (2009) Wood Sci Technol 43:423